Lamb shifts and hyperfine structure in $^6Li^+$ and $^7Li^+$: Theory and experiment

E. Riis and A. G. Sinclair
Department of Physics and Applied Physics, Strathclyde University, Glasgow G4 0NG, Scotland, United Kingdom

O. Poulsen
Mikroelektronik Centret, Danmarks Tekniske Hoejskole, 2800 Lyngby, Denmark

G. W. F. Drake
Department of Physics, University of Windsor, Windsor, Ontario, Canada N9B 3P4

W. R. C. Rowley and A. P. Levick
National Physical Laboratory, Teddington, Middlesex TW11 0LW, England, United Kingdom
(Received 22 July 1993)

High-precision laser-resonance measurements accurate to ±0.5 MHz or better are reported for transitions among the $1s2s\ ^3S_1$–$1s2p\ ^3P_J$ hyperfine manifolds for each of $J = 0$, 1, and 2 in both $^6Li^+$ and $^7Li^+$. A detailed analysis of hyperfine structure is performed for both the S and P states, using newly calculated values for the magnetic dipole and electric quadrupole coupling constants, and the hyperfine shifts subtracted from the measurements. The resulting transition frequencies are then analyzed on three different levels. First, the isotope shifts in the fine-structure splittings are calculated from the relativistic reduced mass and recoil terms in the Breit interaction, and compared with experiment at the ±0.5-MHz level of accuracy. This comparison is particularly significant because J-independent theoretical uncertainties reduce through cancellation to the ±0.01-MHz level. Second, the isotope shifts in the full transition frequencies are used to deduce the difference in rms nuclear radii. The result is $R_{\rm rms}(^6{\rm Li}) - R_{\rm rms}(^7{\rm Li}) = 0.15 \pm 0.01$ fm, in agreement with nuclear scattering data, but with substantially improved accuracy. Third, high-precision calculations of the low-order non-QED contributions to the transition frequencies are subtracted from the measurements to obtain the residual QED shifts. The isotope-averaged and spin-averaged effective shift for $^7Li^+$ is $37\,429.40 \pm 0.39$ MHz, with an additional uncertainty of ±1.5 MHz due to finite nuclear size corrections. The accuracy of 11 parts per million is the best two-electron Lamb shift measurement in the literature, and is comparable to the accuracies achieved in hydrogen. Theoretical contributions to the two-electron Lamb shift are discussed, including terms of order $(\alpha Z)^4$ recently obtained by Chen, Cheng, and Johnson [Phys. Rev. A **47**, 3692 (1993)], and the results used to extract a QED shift for the $2\ ^3S_1$ state. The result of $30\,254 \pm 12$ MHz is shown to be in good accord with theory ($30\,250 \pm 30$ MHz) when two-electron corrections to the Bethe logarithm are taken into account by a $1/Z$ expansion method.

PACS number(s): 35.10.Fk, 31.20.Di, 31.30.Jv

I. INTRODUCTION

Since the pioneering work of Lamb on the measurement of the $2s_{1/2}$-$2p_{1/2}$ transition in hydrogen [1], a wide range of experimental tests of the predictions of quantum electrodynamics (QED) has been carried out. The difficulties involved in accurate calculations of the QED effects have traditionally limited the experimental interest to only the structurally most simple systems. In addition to extending Lamb's work to higher accuracy [2] and to the heavier hydrogenic systems [3,4], this has included the measurement of the $g-2$ factor for single leptons [5], the ground-state hyperfine splitting for hydrogen [6,7] with the possibility of extension to its cousins muonium and positronium [8], as well as precision measurements of the hydrogen $1s$-$2s$ two-photon transition [9].

In the slightly more complicated two-electron systems, the Lamb shift no longer manifests itself as a splitting of otherwise degenerate levels, but rather as a slight shift on top of a large nonrelativistic value with additional significant corrections for relativistic effects, and mass polarization and relativistic recoil. However, very accurate variational techniques exist for obtaining nonrelativistic wave functions allowing these terms to be calculated with better accuracy than the best experiments [10–12]. One of the inherent attractions of the He-like systems is the relatively long lifetime of the $2\ ^3P$ levels. This allows one to benefit from the Z^4 scaling (for low Z) of the one-electron Lamb shift in going to heavier elements. The $2\ ^3P_J$ level widths increase only in proportion to Z up until about $Z = 8$, where singlet-triplet mixing starts quenching the $^3P_1$ level. This is in sharp contrast to a hydrogenlike system where the ratio of the linewidth to the Lamb shift is only weakly dependent on Z and is roughly 10% of the Lamb shift. In the case of Li^+, the

$2\,^3S_1$–$2\,^3P_2$ Lamb shift is about 37 GHz, while the natural linewidth is only 3.7 MHz.

The interpretation of high-precision measurements in He-like ions in terms of QED shifts depends critically upon an accurate knowledge of all lower-order contributions to the energy. An accuracy of ±1 MHz in the Lamb shift corresponds to $\pm 1.5 \times 10^{-10}$ atomic units (a.u.). To this degree of accuracy, the necessary low-order terms that must be subtracted can be written in the form

$$E_{\rm low} = \Big[\varepsilon_{0,0} + \varepsilon_{0,1}(\mu/M) + \varepsilon_{0,2}(\mu/M)^2 + \varepsilon^{(J)}_{2,0}\alpha^2 + \varepsilon^{(J)}_{2,1}\alpha^2(\mu/M) + E_{\rm nuc}\Big] 2R_M, \qquad (1)$$

where α is the fine-structure constant, μ/M is the ratio of reduced electron mass to nuclear mass M, $R_M = (1-\mu/M)R_\infty$ is the finite mass Rydberg, and $\mathbf{J} = \mathbf{L} + \mathbf{S}$ is the total electronic angular momentum. Here, $\varepsilon_{0,0}$ is the nonrelativistic energy for infinite nuclear mass, $E_{\rm nuc}$ is the finite nuclear size correction, and the other terms are discussed in detail in Sec. III C. The older calculations of Pekeris and co-workers [13], which for many years stood as the standard references for $\varepsilon_{0,0}$, $\varepsilon_{0,1}$, and $\varepsilon^{(J)}_{2,0}$, have now been supplanted by much more accurate calculations based on doubled basis sets in Hylleraas coordinates [10–12], or basis sets which include logarithmic terms [14]. The methods of calculation are described in detail in the foregoing references. The results presented in Refs. [10–12] for neutral helium are extended in this paper to Li^+, with an accuracy of ±0.2 kHz in the transition energy $\varepsilon_{0,0}$, and ±3 kHz in the relativistic corrections $\alpha^2\varepsilon^{(J)}_{2,0}$. In addition, new results for the second-order mass polarization term $\varepsilon_{0,2}$ and relativistic recoil term $\varepsilon^{(J)}_{2,1}$ are obtained.

The $2\,^3S_1$–$2\,^3P_J$ transitions of the isotope $^7Li^+$ have been studied in several previous less accurate experiments [15–17]. The present work improves on the previous measurements of Riis *et al.* [17] by nearly an order of magnitude to better than ±0.5 MHz. The improved accuracy is obtained by using a fast ion beam in conjunction with the techniques of Lamb dip spectroscopy with two dye lasers referenced to saturated absorption lines in iodine. In addition, measurements are reported for both isotopes $^6Li^+$, with nuclear spin $I = 1$, and $^7Li^+$ with $I = 3/2$. The hyperfine structure of the $2\,^3S_1$ state has been measured previously for both isotopes [18], but these are the first high-precision measurements to determine the isotope shift in the $2\,^3S_1$–$2\,^3P_J$ transition frequencies. Results are reported for a single hyperfine component in each of the $J = 0$, 1, and 2 manifolds.

Recent work by Rong *et al.* [19] has attained a quoted precision of ±2 MHz in the fine-structure splittings of $^7Li^+$ by heterodyne laser spectroscopy; but their intervals differ from ours by as much as 17 MHz. Their results are further discussed in Sec. III E. Somewhat lower precision measurements for He-like ions in the low-Z region are available for Be^{2+} (±12 MHz) [20], and B^{3+} (±390 MHz) [21]. Results for the entire range of Z have recently been discussed by Berry, Dunford, and Livingston [22] and compared with the unified calculations of Drake [23]. This discussion will not be repeated here; but additional comments on and extensions of the unified method to include the recent calculations of Chen, Cheng, and Johnson [24] are contained in Sec. III D.

Our measurements on both isotopes $^6Li^+$ and $^7Li^+$ allow the results to be interpreted on several different levels. First, it is evident from Eq. (1) that differences in isotope shifts for different J values are determined almost entirely by the terms

$$\left[\varepsilon^{(J)}_{2,0}\alpha^2 + \varepsilon^{(J)}_{2,1}\alpha^2(\mu/M)\right] 2R_M,$$

since only these depend on both μ/M and J. In the absence of hyperfine structure, the comparison with theory would remain significant down to the level of a few kHz because uncertainties due to QED and finite nuclear size corrections cancel on taking differences of isotope shifts for different J values. We will call this the splitting isotope shift (SIS). Second, the consistency of the isotope shifts for different J's provides a check on the calculated hyperfine-structure corrections. Third, the isotope shift itself provides a precise measure of the relative nuclear sizes, since the change in $E_{\rm nuc}$ in Eq. (1) for the two isotopes is then determined. Finally, the total transition frequencies for each isotope provide a measure of the remaining QED shift after the other terms in Eq. (1) have been subtracted.

The paper is organized as follows. Section II describes the details of the laser-induced flourescence method used to obtain high-precision measurements of the transition frequencies, and their calibration against I_2 reference lines. In Sec. III, the hyperfine shifts are first calculated and compared with experiment, using a semiempirical method to determine the dominant Fermi contact term. These shifts are then subtracted from the measurements, and the remaining transition frequencies analyzed in terms of SIS, total isotope shifts, and QED shifts. Finally, theoretical contributions to the QED shifts are discussed and compared with experiment. Section IV discusses the results obtained at the three levels of analysis, and in particular relates the measurements to recent and ongoing QED calculations.

II. EXPERIMENTAL

As with the previous measurement of the $2\,^3S$–$2\,^3P$ transition in Li^+ [17], this experiment uses laser-induced fluorescence from a fast ion beam traveling colinearly with the laser beams. However, whereas that experiment measured the red- and blue-shifted Doppler broadened transitions with co- and counterpropagating laser beams separately, we have in this experiment used two lasers and observed the saturated fluorescence signal from the beam as both laser beams are Doppler shifted into resonance with the same hyperfine transition. There are several advantages to this technique. First, we do not have to worry about slight variations in the beam velocity between individual blue and red shifted measurements. Second, the

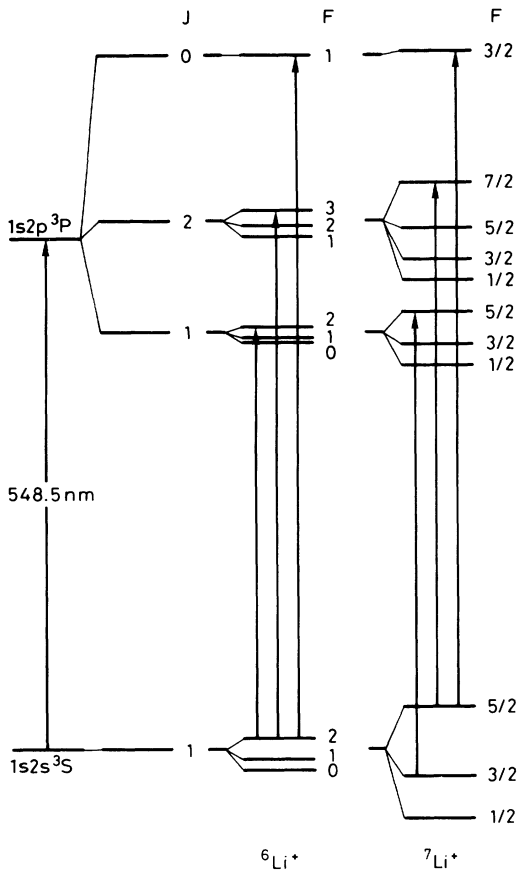

FIG. 1. Fine and hyperfine structures for the $1s2s\,^3S$ and $1s2p\,^3P$ levels of $^7Li^+$ and $^6Li^+$. The three transitions for each isotope indicated by arrows are the ones measured in this experiment.

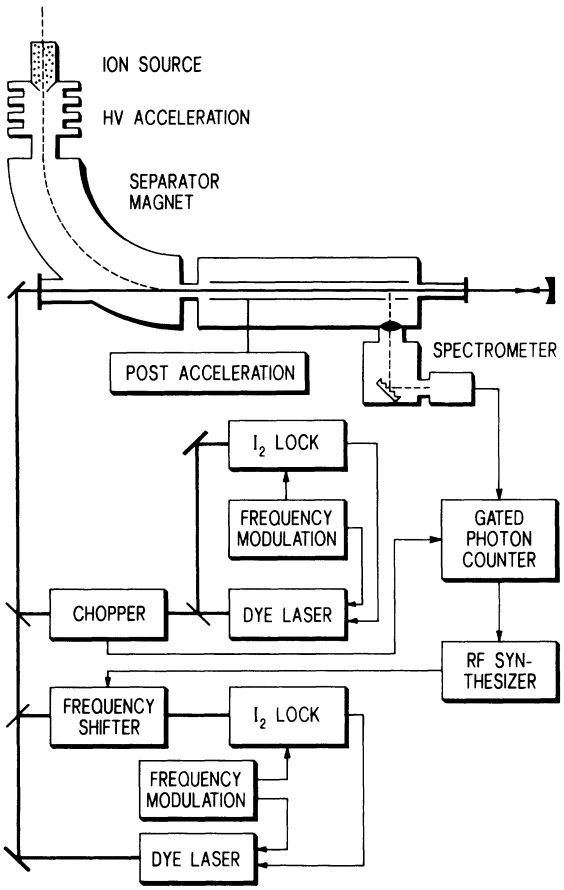

FIG. 2. The experimental setup consists of an accelerator and two dye lasers locked and offset locked, respectively, to saturated absorption lines in I_2 vapor. A mechanical chopper in the fixed frequency laser beam allows the ion beam fluorescence to be recorded with both lasers on and with the scanning laser only.

measured line is narrower and its shape is to first order insensitive to the velocity distribution of the ions. As with the previous experiment, a hyperfine transition to each of the three fine-structure levels was measured relative to saturated absorption lines in I_2. The fine and hyperfine structures for the $2\,^3S$–$2\,^3P$ transitions in both isotopes are shown in Fig. 1. Also indicated are the measured hyperfine components. A subsequent determination of the absolute frequencies of a total of nine I_2 lines completed the measurement.

A. The fast-beam experiment

The experimental setup is shown schematically in Fig. 2. The ions are produced in a universal discharge ion source where LiCl is heated to 400–500 °C. In order to obtain sufficient beam current in the $^6Li^+$ experiment, LiCl enriched to > 95% in this isotope was used. A small fraction of the ions leaves the source in the metastable $2\,^3S_1$ state and with a slightly lower energy than the ground-state ions. The low energy spread of the ion source combined with the stability of the acceleration voltage results in an approximately 100-MHz-wide Doppler profile after an acceleration to 100 kV. A 90° bending magnet selects the isotope and a post acceleration in the following straight section provides a convenient finetuning of the beam velocity. The fluorescence from the beam is detected with a spectrometer and a photomultiplier.

The dye laser exiting the beam in the copropagating geometry (the pump beam) is locked to a saturated I_2 absorption line. The other dye laser is tuned into resonance with the ion beam in the counterpropagating geometry. A part of this laser beam is frequency shifted by 400–600 MHz using an acousto-optic modulator in a double pass geometry, thus eliminating angular deflection to first order. The frequency shifted beam is locked to a saturated I_2 absorption line. By varying the applied drive frequency to the acousto-optic modulator, this laser (the probe) is scanned across the Doppler profile with rf precision.

Before entering the accelerator, the pump beam is chopped by a mechanical chopper. This allows simultaneous recordings of the absorption profile with the probe laser only, and with both lasers. Figures 3(a) and 3(b) show an example of simultaneous scans of the probe beam with and without the pump beam. The difference shown

in Fig. 3(c) displays the saturated signal on a constant background due to the fluorescence induced by the pump. In order to allow the most accurate determination of the frequency of this nonlinear signal, the beam velocity is chosen so that it appears close to the center of the Doppler profile. From the recorded difference spectra, the offset frequency is determined with an accuracy (one standard deviation) of typically less than 500 kHz. The systematic error introduced by an angular misalignment of the two laser beams relative to the ion beam is estimated to cause an error of less than 250 kHz in the final result.

During this part of the experiment the I_2 reference lines were identified using the I_2 atlas [25] and their absolute transition frequencies were determined with a wave meter. An independent wave meter measurement later confirmed these results. With an accuracy of better than 30 MHz, these measurements were sufficient for a subsequent interferometric calibration to yield an unambiguous absolute value for the frequencies of the saturated I_2 lines.

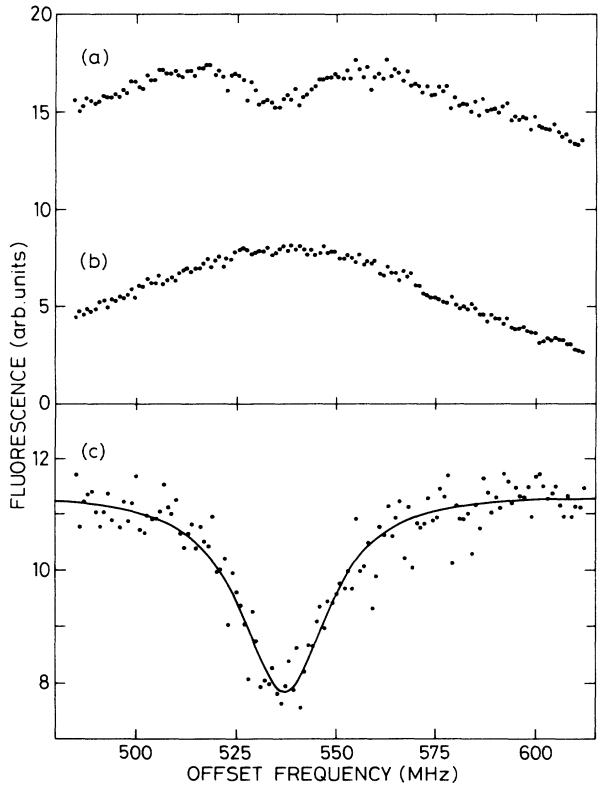

FIG. 3. Simultaneous recordings of the fluorescence from the ion beam with (a) both lasers and (b) probe laser only tuned to the $1s2s\,^3S_1$, $F = 2$ to $1s2p\,^3P_0$, $F = 1$ transition in $^6Li^+$. The difference isolating the Lamb dip is shown in (c) together with the fitted curve. The expected line shape of the saturated signal is the power broadened natural line shape normalized with the velocity profile. The fitted curve is therefore a Lorentzian multiplied with a Gaussian whose width and position are determined by the probe spectrum (b).

B. The I_2 calibration

Both dye lasers in the fast-beam experiment, as well as the one used in the subsequent calibration, were locked to saturated absorption lines in iodine to ensure long term stability, as well as high absolute frequency accuracy. The saturated absorption lines were observed by subtracting the intensities of two balanced probe beams, one of which overlapped the counterpropagating pump beam. By frequency modulating the laser at a rate of ~18 kHz and an amplitude of ~ 500 kHz and demodulating the difference in intensity between the two probe beams, first derivative lines were obtained with a linewidth of ~ 1.5 MHz. A typical spectrum is shown in Fig. 4. The two probe beams result in an efficient suppression of the Doppler background. This is important in order to ensure that the lasers are reproducibly locked to the center of the saturated absorption lines. The locks were established by feeding the time integral of the demodulated difference signal back to the lasers with a proper phase. The stability of the locks was investigated by counting the beat frequency of the two lasers when they were locked and offset locked, respectively, to the same I_2-saturated absorption line and comparing it with the frequency applied to the acousto-optic modulator. The reproducibility was found in this way to be better than 5 kHz. The I_2 cell was maintained at a temperature of 0 °C throughout the experiment, thus reducing the pressure shift in the cell to about 30 kHz, as well as keeping it constant.

The absolute calibration, carried out using a 1 m evacuated plane-plane Fabry-Pérot resonator referenced to an I_2-stabilized He-Ne laser, was similar to previously reported calibrations [26]. The interferometer was locked to the I_2 stabilized dye laser and a He-Ne laser was in turn locked to the interferometer. The beat frequency between this laser and an I_2-stabilized He-Ne laser was counted. This frequency difference combined with the integer interferometer order number for the dye laser gave the absolute dye laser frequency. Two to four series of measurements consisting of 20 determinations of the difference frequency were carried out on each line. One important difference from previously reported calibrations, however, is that this time we have used the

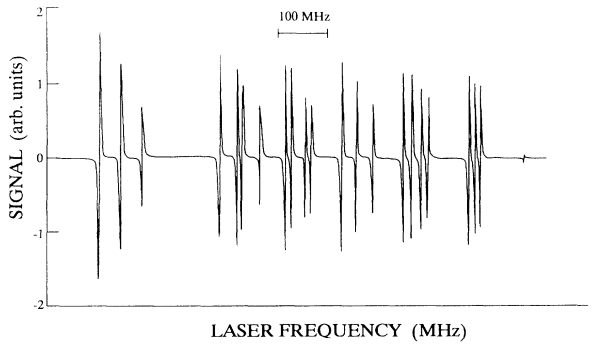

FIG. 4. Saturated absorption spectrum of the hyperfine components of line no. 4526 in the I_2 atlas [25]. The scan width is 1 GHz.

TABLE I. The effects of the various sources of systematic errors in the calibration process on the final values for the absolute frequencies for the Li^+ transitions.

Source of error	Standard deviation (kHz)
633 nm reference	14
Phase shift determination	16
Flatness and illumination uniformity	36
Prismatic imbalance (image shear)	33
Servo errors, interferometer	11
Servo errors, I_2 lock	15
Statistical repeatability	112
Total (root sum of squares)	121

TABLE II. The absolute transition frequencies for the measured Li^+ hyperfine components. The quoted error is the statistical error from 9 to 13 measurements of the rf offset frequency combined with a 280 kHz systematic error from the saturated fluorescence experiment and the calibration procedure.

Isotope	Transition $(J,F) \rightarrow (J',F')$	Frequency (MHz)
$^6Li^+$	$(1,2) \rightarrow (0,1)$	546 522 996.76(36)
	$(1,2) \rightarrow (1,2)$	546 368 567.96(44)
	$(1,2) \rightarrow (2,3)$	546 432 721.98(43)
$^7Li^+$	$(1,5/2) \rightarrow (0,3/2)$	546 549 605.65(42)
	$(1,3/2) \rightarrow (1,5/2)$	546 417 348.12(51)
	$(1,5/2) \rightarrow (2,7/2)$	546 466 918.79(40)

recently recommended value for the absolute frequency of the reference He-Ne laser [27] and have therefore obtained a significant increase in accuracy. The complete error budget for the calibration is shown in Table I. The interferometer phase shift was obtained by extrapolation from previous measurements at 486 nm. The accuracy of the I_2 lock is in this part of the experiment taken to be 15 kHz.

III. THEORETICAL ANALYSIS

The absolute frequencies ν_0 for the Li^+ transitions are now determined as

$$\nu_0 = \sqrt{\nu_R \nu_B}, \tag{2}$$

where ν_R and ν_B are the absolute frequencies for the red- and blue-shifted probe and pump frequencies, respectively. The measured values are shown in Table II.

A. Hyperfine structure

The next step towards determining Li^+ fine-structure energies is to remove the rather large hyperfine structure from the measured frequencies. Since only a single hyperfine component is measured for each J of the $1s2p\,^3P_J$ states, the final results depend strongly on the accuracy of this part of the calculation. A careful analysis is required of all possible contributions, including off-diagonal matrix elements mixing states of different S. Defining

$$W^{I,F}_{J,J'}(K) = (-1)^{J+I+F}[(2J+1)(2J'+1)]^{1/2} \times \begin{Bmatrix} F & I & J' \\ K & J & I \end{Bmatrix} \Big/ \begin{pmatrix} I & K & I \\ -I & 0 & I \end{pmatrix}, \tag{3}$$

and

$$X_{S,S'} = -[(2S+1)(2S'+1)]^{1/2} \begin{Bmatrix} 1/2 & S' & 1/2 \\ S & 1/2 & 1 \end{Bmatrix}, \tag{4}$$

then, using the sign conventions of Edmonds [28] for off-diagonal terms, the magnetic dipole and electric quadrupole hyperfine-structure matrix elements in the coupled representation are [29]

$$\begin{aligned} \langle (L'S')J'IF|H_{\rm hyp}|(LS)JIF\rangle = W^{I,F}_{J,J'}(1) \Bigg[& C_{S',S}\delta_{L',L}\sqrt{6}(-1)^{L+J'} X_{S,S'} \begin{Bmatrix} S' & J' & L \\ J & S & 1 \end{Bmatrix} \\ & - D_S \delta_{S,S'} (-1)^{J+S+M} \begin{Bmatrix} L' & J' & S \\ J & L & 1 \end{Bmatrix} \Big/ \begin{pmatrix} L' & 1 & L \\ -M & 0 & M \end{pmatrix} \\ & + E_{S',S} \frac{12}{\sqrt{5}} (-1)^{S'-L'+M} X_{S,S'} \begin{Bmatrix} L' & L & 2 \\ S' & S & 1 \\ J' & J & 1 \end{Bmatrix} \Big/ \begin{pmatrix} L' & 2 & L \\ -M & 0 & M \end{pmatrix} \Bigg] \\ & + \tfrac{1}{4} W^{I,F}_{J,J'}(2) Q_S \delta_{S',S} (-1)^{J+S+M} \begin{Bmatrix} L' & J' & S \\ J & L & 2 \end{Bmatrix} \Big/ \begin{pmatrix} L' & 2 & L \\ -M & 0 & M \end{pmatrix}, \end{aligned} \tag{5}$$

expressed in terms of 3-j, 6-j, and 9-j symbols. The last term is the electric quadrupole matrix element. The definitions for the structure-dependent constants [30,31], extended to include off-diagonal matrix elements, are

$$C_{S',S} = -\frac{8\pi}{3} g_I \mu_0^2 \langle \gamma',\ ^{2S'+1}LM \mid \delta(\mathbf{r}_1) + (-1)^{S'-S}\delta(\mathbf{r}_2) \mid \gamma,\ ^{2S+1}LM \rangle\ , \tag{6}$$

$$D_S = -2 g_I \mu_0^2 \langle \gamma',\ ^{2S+1}L'M \mid l_{1,z} r_1^{-3} + l_{2,z} r_2^{-3} \mid \gamma,\ ^{2S+1}LM \rangle\ , \tag{7}$$

$$E_{S',S} = -\tfrac{5}{2} g_I \mu_0^2 \langle \gamma',\ ^{2S'+1}L'M \mid (-1)^{S'-S} C_2^0(\hat{\mathbf{r}}_1) r_1^{-3} + C_2^0(\hat{\mathbf{r}}_2) r_2^{-3} \mid \gamma,\ ^{2S+1}LM \rangle\ , \tag{8}$$

evaluated with $M = L$ throughout Eqs. (5)–(8). Here, $C_2^0(\hat{\mathbf{r}}) = \sqrt{4\pi/5}\, Y_2^0(\hat{\mathbf{r}})$, $\boldsymbol{l}_i = \mathbf{r}_i \times \mathbf{p}_i$, and μ_0 is the Bohr magneton. Using $\boldsymbol{\mu} = -g_I \mu_0 \mathbf{I}$, the atomic beam magnetic resonance measurements of Beckmann, Böklen, and Elke [32] yield $g_I = -4.477\,009(3) \times 10^{-4}$ and $-1.182\,3370(8) \times 10^{-3}$ for ^{6}Li ($I = 1$) and ^{7}Li ($I = 3/2$), respectively. These values include a diamagnetic shielding correction as tabulated by Raghavan [33]. They differ from the older measurements of Lutz [34] at the parts in 10^5 level due to chemical shifts in their NMR data [32]. The conversion factors from a.u. to MHz are thus $g_I \mu_0^2 = -39.216\,04(3)$ MHz a_0^3 and $-103.5660(7)$ MHz a_0^3 for the two cases. Finally, the electric quadrupole coupling constant Q_S is related to $E_{S,S}$ by

$$Q_S = -E_{S,S}\left(\frac{16IQ}{5 g_I \alpha^2 a_0^2}\right)\ , \tag{9}$$

where Q is the electric quadrupole moment, and $a_0 \simeq 0.529\,177 \times 10^{-8}$ cm is the Bohr radius. The quadrupole moments are $-0.000\,83(8) \times 10^{-24}$ cm^2 for ^{6}Li [35], and $-0.0370(8) \times 10^{-24}$ cm^2 for ^{7}Li [36].

We have calculated high precision values for all the matrix elements in Eqs. (6)–(8), using the double-basis-set wave functions in Hylleraas coordinates described previously [10–12]. Mass polarization corrections to the wave functions are included, and the term linear in μ/M extracted. The final results are then expressed in the forms

$$C_{S',S} = C^{(0)}_{S',S}[1 + (\delta^C_{\rm MP} - 3)\mu/M + \alpha/2\pi + \delta^C_{\rm HO}]\ , \tag{10}$$

$$D_S = D^{(0)}_S[1 + (\delta^D_{\rm MP} - 3)\mu/M + \delta^D_{\rm HO}]\ , \tag{11}$$

$$E_{S',S} = E^{(0)}_{S',S}[1 + (\delta^E_{\rm MP} - 3)\mu/M + \alpha/2\pi + \delta^E_{\rm HO}]\ , \tag{12}$$

where $\delta_{\rm MP}$ is the mass polarization correction coefficient for each term, $-3\mu/M$ is the reduced mass correction, and $\delta_{\rm HO}$ represents higher order relativistic, QED, and finite nuclear size corrections. The results are summarized in Table III. The last two columns include all terms up to $\delta_{\rm HO}$. Note that for D_1 and $E_{1,1}$, the mass polarization corrections and reduced mass corrections nearly cancel. The values of μ/M are $9.121\,677 \times 10^{-5}$ for ^{6}Li and $7.820\,203 \times 10^{-5}$ for ^{7}Li [37] (including binding energy corrections).

The hyperfine shifts are dominated by the Fermi contact term $C_{1,1}$. In order to achieve sufficient precision for this term, it is necessary to estimate the contribution from $\delta^C_{\rm HO}$ in Eq. (10). This is difficult to do directly because of nuclear structure and QED uncertainties. The argument suggested by Hambro [30] and used by Hinds, Prestage and Pichanick [31] is to assume that for the P states, $\delta^C_{\rm tot}(1s2p) \simeq \delta^C_{\rm tot}(1s)$ where $\delta^C_{\rm tot}(1s)$ is the total anomaly [i.e., the sum of the corrections in Eq. (10)] for the corresponding one-electron ion. The justification is that the anomaly comes predominantly from the $1s$ electron. We can now do somewhat better than this by assuming instead that $\delta^C_{\rm HO}(1s2p) \simeq \delta^C_{\rm HO}(1s)$, since the $\delta^C_{\rm MP}$ contribution in Eq. (10) is known and can be subtracted out. Unfortunately, high precision hyperfine splitting measurements are not available to our knowledge for $Li^{2+}(1s)$. However, data for the $Li^+(1s2s\,^3S_1)$ state can be used instead if a correction is made for the $2s$ electron. The details are given in the following paragraphs.

For the $2\,^3S_1$ state, the splittings have been measured to an accuracy of better than ± 50 kHz for both isotopes, using microwave spectroscopy [18]. The next step is to compare these splittings with theory. For S states, the $C_{1,1}$ and $C_{1,0}$ terms are the only important contributions, with $C_{1,0}$ inducing an off-diagonal mixing with the $2\,^1S_0$ state. The calculated diagonal singlet-triplet splittings are 459 860 GHz for $^6Li^+$ and 459 865 GHz for $^7Li^+$. The results in Table IV show the best fit to the data with $C_{1,1}$ as an adjustable parameter. For $^7Li^+$, including the off-diagonal $C_{1,0}$ term changes the splittings by ± 0.372 MHz, and markedly improves the agreement with experiment. For $^6Li^+$, the changes are only ± 0.028 MHz and agreement with experiment remains about the same.

The point of this comparison is that the experimental and theoretical values for $C_{1,1}$ are significantly different. If this difference is attributed to $\delta^C_{\rm HO}$, then, in parts per million (ppm)

$$\delta^C_{\rm HO}(^6Li^+, 2\,^3S_1) = 131(6)\ \text{ppm}\,, \tag{13a}$$

TABLE III. Calculated values of the $^6Li^+$ and $^7Li^+$ hyperfine-structure coefficients for the $1s2s\,^3S$, $1s2s\,^1S$, $1s2p\,^3P$, and $1s2p\,^1P$ states. The subscripts are the spin labels S' and S. The last two columns include the finite nuclear mass and anomalous magnetic moment correction factors shown in Eqs. (10)–(12), but not $\delta_{\rm HO}$.

Coeff.	Zero order ($g_I\mu_0^2$)	$\delta_{\rm MP}$	Total (MHz) ^{6}Li	Total (MHz) ^{7}Li
S states				
$C_{1,1}$	−76.467 138	0.0015	3001.400	7926.729
$C_{1,0}$	−65.126 038	−0.0120	2556.252	6751.089
P states				
$C_{1,1}$	−70.959 167	−0.0761	2785.188	7355.721
$C_{1,0}$	−71.263 413	−0.1404	2797.113	7387.220
D_1	−0.959 417	3.0726	37.625	99.363
D_0	−0.621 665	−3.1002	24.366	64.353
$E_{1,1}$	0.243 753	2.60	−9.570	−25.273
$E_{1,0}$	0.202 587	−0.309	−7.951	−21.000
Q_1			−0.038(4)	−1.70(4)

TABLE IV. Comparison of theory and experiment [18] for the hyperfine splittings of the $1s2s\,^3S_1$ state of $^6Li^+$ and $^7Li^+$. The last two columns compare theory with and without the singlet-triplet hyperfine mixing term $C_{1,0}$. Units are MHz.

		Theory	
Transition	Experiment	With $C_{1,0}$	Without $C_{1,0}$
^{6}Li, $F = 0 \to 1$	3 001.780(50)	3 001.765	3001.793
^{6}Li, $F = 1 \to 2$	6 003.600(50)	6 003.614	6003.586
^{6}Li, $C_{1,1}$	3 001.793(17)	3 001.400	
^{7}Li, $F = 1/2 \to 3/2$	11 890.018(40)	11 890.013	11 890.385
^{7}Li, $F = 3/2 \to 5/2$	19 817.673(40)	19 817.679	19 817.308
^{7}Li, $C_{1,1}$	7 926.923(14)	7 926.729	

$$\delta^C_{\rm HO}(^7{\rm Li}^+, 2\,^3S_1) = 25(2)\ {\rm ppm}\,. \tag{13b}$$

These anomalies also come largely from the $1s$ electron, and agree in order of magnitude with the known terms given by [8]

$$\delta^C_{\rm HO}(1s) = \delta_{\rm rel}(1s) + Z\alpha^2(\ln 2 - \tfrac{5}{2}) - 2Z\langle R_{\rm em}\rangle/a_0 + \delta'_{\rm HO}, \tag{14}$$

where

$$\delta_{\rm rel}(1s) = \tfrac{3}{2}(Z\alpha)^2 \tag{15}$$

is the Breit relativistic correction for the $1s$ electron, $\langle R_{\rm em}\rangle$ is an average electromagnetic charge radius for the nucleus (the Zemach term, [38,8]), and

$$\delta'_{\rm HO} = -\frac{8\alpha}{3\pi}(Z\alpha)^2 \ln Z\alpha \left(\ln Z\alpha - \ln 4 + \tfrac{281}{480}\right) + \frac{\alpha}{\pi}(Z\alpha)^2(15.38 \pm 0.29)\,. \tag{16}$$

The contributions from the terms in Eq. (14) are 719, -289, ~ -380, and -35 ppm, respectively, for a total of 15 ppm. The Zemach contribution of ~ -380 ppm is only an estimate which depends on the details of the electric charge and magnetic dipole distributions of the two isotopes. Even so, the difference in anomalies of 106(6) ppm between the two isotopes is suprisingly large. Assuming equal Gaussian distributions for the electric charge and magnetic dipole distributions, then $\langle R_{\rm em}\rangle$ is related to the rms nuclear radius $R_{\rm rms}$ by [38]

$$\langle R_{\rm em}\rangle = 4R_{\rm rms}/\sqrt{3\pi}. \tag{17}$$

A rather large adjustment would have to be made for one of the isotopes from the assumed value of $\langle R_{\rm em}\rangle = 3.35$ fm ($R_{\rm rms} = 2.57$ fm) [39] in order to resolve the discrepancy. It may be that nuclear polarization is playing a significant role.

We next estimate the contribution of the $2s$ electron to the $\delta^C_{\rm HO}(2\,^3S_1)$ values in Eqs. (13a) and (13b). Since the effect is small, a rough estimate will suffice. The contribution comes primarily from $\delta_{\rm rel}(2s)$ given by

$$\delta_{\rm rel}(2s) = \tfrac{51}{24}(Z\alpha)^2 \tag{18}$$

in a one-electron approximation. As a point of reference, the effect of the $2s$ electron can be seen directly in the case of ^{3}He by comparing the total hyperfine structure anomalies for $^3{\rm He}(2\,^3S_1)$ and $^3{\rm He}^+(1s)$. The details are summarized in Table V. The small difference in the anomalies of 3.8(3) ppm represents the change in $\delta^C_{\rm HO}$ due to the $2s$ electron after the extraneous effects of mass polarization and singlet-triplet mixing have been accounted for. This value is in harmony with the semi-empirical formula

$$\delta^C_{\rm HO}(1sns) - \delta^C_{\rm HO}(1s) \simeq \left\{ \frac{\delta_{\rm rel}(1s) + n^{-3}[(Z-1)/Z]^2\delta_{\rm rel}(ns)}{1 + n^{-3}[(Z-1)/Z]^2} - \delta_{\rm rel}(1s) \right\}, \tag{19}$$

which for $n = 2$ reduces to

$$\delta^C_{\rm HO}(1s2s) - \delta^C_{\rm HO}(1s) \simeq \frac{15}{192}\left\{\frac{(Z-1)^2\alpha^2}{1 + \frac{1}{8}[(Z-1)/Z]^2}\right\} = 4.0\ {\rm ppm\ for}\ Z = 2\,. \tag{20}$$

TABLE V. Comparison of hyperfine splittings and anomalies for $^3{\rm He}(2\,^3S_1)$ and $^3{\rm He}^+(1s)$, using $g_I = 2.317\,4824(7) \times 10^{-3}$ [53] and $g_I\mu_0^2 = 202.998\,21(7)$ MHz a_0^3. For the singlet-triplet mixing term, $C_{1,0} = -3945.046$ MHz, and the diagonal singlet-triplet splitting is 192 502.7 GHz. The mass polarization correction factor for $C^0_{1,1}$ is $(1 + 0.001\,649\mu/M)$ with $\mu/M = 1.819\,212\,04 \times 10^{-4}$. Units are MHz.

Term	$^3{\rm He}(2\,^3S_1)$	$^3{\rm He}^+(2s_{1/2})$
$C^0_{1,1}$	$-4490.8810(14)$[a]	$-4330.6284(14)$[a]
Zero-order splitting	6736.3215(21)	8661.2568(28)
Mass polarization	-0.00203	0
Singlet-triplet mixing	0.06063	0
Total splitting	6736.2588(21)	8661.2568(28)
Measured splitting	6739.701177(16)[b]	8665.64987(1)[c]
Anomaly	511.0(3) ppm	507.2(3) ppm

[a] Uncertainty due to g_I.
[b] Rosner and Pipkin, Ref. [54].
[c] Schuessler, Fortson, and Dehmelt, Ref. [55].

Similar formulas have proven useful in calculating other two-electron properties which are proportional to the electron density at the nucleus, such as the Lamb shift [10–12]. For Li^+ ($Z = 3$), the predicted anomaly difference from Eq. (20) scales up to 16 ppm. Subtracting this correction from Eqs. (13a) and (13b) then yields

$$\delta^C_{\rm HO}(^6{\rm Li}^{2+}, 1s) = 115(16)\ {\rm ppm}\,, \tag{21a}$$
$$\delta^C_{\rm HO}(^7{\rm Li}^{2+}, 1s) = 9(16)\ {\rm ppm}\,, \tag{21b}$$

where the entire amount of the correction has been taken as the uncertainty.

The $2p$ electron also has one-electron relativistic corrections of $\delta_{\rm rel}(2p_{1/2}) = \frac{47}{24}(Z\alpha)^2$ and $\delta_{\rm rel}(2p_{3/2}) = \frac{7}{24}(Z\alpha)^2$; but these apply to the much smaller terms D_S and $E_{S',S}$, rather than to $C_{S',S}$, and are therefore negligible. With this in mind, we assume that $\delta^C_{\rm HO}(1s2p) = \delta^C_{\rm HO}(1s)$, and obtain the corrected values of $C_{1,1}$ for the $1s2p\,^3P$ states of Li^+ as

$$C_{1,1}(^6{\rm Li}^+) = 2785.51(4)\ {\rm MHz}\,, \tag{22a}$$
$$C_{1,1}(^7{\rm Li}^+) = 7355.78(12)\ {\rm MHz}\,, \tag{22b}$$

in place of the entries in the last two columns of Table III.

For $^7Li^+$, the above result agrees with the value 7355.44(39) MHz obtained from our least-squares fit to the hyperfine splittings measured by Kowalski *et al.* [18] with $C_{1,1}$, D_1, and $E_{1,1}$ as adjustable parameters. However, these authors have not discussed the possibility for systematic shifts of the microwave transition frequency by the presence of a near-resonant laser field. There appear to be small but significant discrepancies for D_1 and $E_{1,1}$. The results of the fit are $D_1 = 100.29(52)$ MHz and $E_{1,1} = -24.77(5)$ MHz, as compared with the theoretical values 99.363 and −25.273 MHz, respectively, in Table III.

With these values for $C_{1,1}$, together with the other input data in Tables III and VI, the hyperfine shifts can now be calculated by diagonalizing the complete fine- and hyperfine-structure matrix. The results are shown in Table VII. The final uncertainties are dominated by the $C_{1,1}$ uncertainties. For $^7Li^+$, the nuclear electric quadrupole moment has a significant effect. For the relevant ^3P hyperfine states $(J,F) = (0,3/2)$, $(1,5/2)$, and $(2,7/2)$, the contributions to the shifts are −0.018, −0.051, and −0.42 MHz, respectively. Finally, combining the calculated shifts with the measured transition frequencies in Table II gives the transition frequencies in Table VIII with hyperfine structure removed. The table also lists the derived isotope shifts for the three transitions.

TABLE VI. Fine-structure parameters used to calculate the $Li^+(1s2p\,^3P_J)$ hyperfine shifts. Following the notation of Hinds, Prestage, and Pichanick [31], the terms are $\Delta = E(2\,^1P_1) - E(2\,^3P_2)$, $E_0 = E(2\,^3P_0) - E(2\,^3P_2)$, $E_1 = E(2\,^3P_1) - E(2\,^3P_2)$, $E_1' = E_1 - E_{st}$ where E_{st} is the singlet-triplet mixing correction, and E_M is the off-diagonal singlet-triplet matrix element. E_0 and E_1 are chosen to be consistent with the intervals derived from the experimental values. Units are MHz.

Parameter	$^6Li^+$	$^7Li^+$
E_0	93 027.04(56)	93 025.84(61)
E_1	−62 676.96(62)	−62 678.29(67)
E_1'	−62 542.72(62)	−62 544.02(67)
E_M	−174 290(50)	−174 294(50)
Δ	226 243×10³	226 199×10³
E_{st}	−134.24(10)	−134.27(10)

TABLE VII. Calculated hyperfine shifts for $Li^+(1s2s\,^3S_1)$ and $Li^+(1s2p\,^3P_J)$. Units are MHz.

$^6Li^+$		$^7Li^+$	
J, F	Shift	J, F	Shift
	$^3S_1$ states		
1, 0	−6003.586(34)	1, 1/2	−19 817.308(35)
1, 1	−3001.821(17)	1, 3/2	−7 927.295(14)
1, 2	3001.793(17)	1, 5/2	11 890.385(21)
	^3P_J states		
0, 1	63.216(2)	0, 3/2	812.965(27)
1, 0	−2867.563(40)	1, 1/2	−9 762.97(16)
1, 1	−1549.914(23)	1, 3/2	−5 524.11(12)
1, 2	1338.413(17)	1, 5/2	4 442.03(5)
2, 1	−4170.415(58)	2, 1/2	−16 432.47(26)
2, 2	−1312.413(17)	2, 3/2	−10 229.20(15)
2, 3	2815.469(40)	2, 5/2	−621.081(12)
		2, 7/2	11 151.97(18)

B. Isotope shifts

The results in Table VIII show that the isotope shifts are slightly different for each of the fine-structure levels. In fact, as pointed out in the Introduction, a comparison between theory and experiment for the *differences* of isotope shifts for different J's is particularly significant because uncertainties due to J-independent QED and finite nuclear size corrections cancel. Only those

TABLE VIII. Experimental results for the $2\,^3S_1$–$2\,^3P_J$ transition frequencies and isotope shifts of Li^+ as obtained from the measured values listed in Table II and the calculated hyperfine shifts in Table VII. The uncertainties are the combined uncertainties from the experimental values and the calculated hyperfine coupling constants.

Isotope	J	Frequency (MHz)
$^6Li^+$	0	546 525 935.34(36)
	1	546 370 231.34(44)
	2	546 432 908.30(43)
$^7Li^+$	0	546 560 683.07(42)
	1	546 404 978.80(51)
	2	546 467 657.21(44)
Isotope shift	0	34 747.73(55)
	1	34 747.46(67)
	2	34 748.91(62)

terms that depend on both J and μ/M contribute to the splitting isotope shifts (SIS). Thus the ^3S state energies cancel exactly from the SIS, while the ^3P states make spin-dependent contributions as summarized in Table IX. Although the totals are small, it is noteworthy that the individual contributions are much larger. The large size of the B_5^X mass polarization correction to the spin-spin interaction is particularly interesting because this term vanishes in the asymptotic limit of high-L Rydberg states [10]. As a check, we have verified that all terms tend to the correct value in the asymptotic limit, as discussed by Drake [11,12], and by Drake and Yan [10].

The contributions to the SIS for $J = 0 \to 1$ and $1 \to 2$ are obtained by multiplying the entries in Table IX by $1 - (\mu/M)_{^6Li}/(\mu/M)_{^7Li} = -0.166\,425$. The results are 0.29 and -2.84 MHz, respectively. The corresponding experimental values from Table VIII are 0.27(87) and $-1.45(91)$ MHz. The $0 \to 1$ SIS is in excellent agreement, but the $1 \to 2$ SIS shows a significant discrepancy of $2.84 - 1.45(91) = 1.39(91)$ MHz. The reason for this is not clear. For example, if δ_{HO}^C for ^{7}Li were increased to reduce the apparent difference of about 100 ppm in the hyperfine anomalies for the two isotopes [see Eqs. (21a) and (21b)], then this would make the above discrepancy worse. Possible contributions from higher-order uncalculated terms can be estimated from the differences between theory and experiment for the total transition frequencies (see Sec. III C). If these differences of about 100 MHz are assumed to scale in proportion to $(1 \pm \mu/M)^6$ (e.g., relativistic terms proportional to p^6), then the implied contribution to the isotope shift is only ± 8 kHz. This can be taken as an indication of the theoretical uncertainty in the calculated SIS. The only other experiment with sufficient accuracy to be sensitive to SIS is that of Zhao, Lawall, and Pipkin [40] for ^{3}He and ^{4}He. There, the measured values of 0.275(38) and $-0.977(38)$ MHz for the same two intervals are in close agreement with theory [11].

TABLE IX. Spin- and mass-dependent contributions to the energies of the $2\,^3P_J$ states of $^7Li^+$. The corresponding entries for $^6Li^+$ are larger by a factor of $(\mu/M)_{^6Li}/(\mu/M)_{^7Li} = 1.166\,425$, and the contributions to the SIS are obtained by multiplying by $-0.166\,425$. $B_{3,Z}$, $B_{3,e}$, and B_5 are the spin-orbit, spin-other-orbit, and spin-spin interactions, respectively, $B_{3,Z}^X$, $B_{3,e}^X$, and B_5^X are the corresponding mass polarization corrections, and Δ_3 is the spin-dependent Stone term [55,10]. The primed terms at the end include only the spin- and mass-dependent parts of each contribution to the total. Units are MHz.

Matrix element	$J = 0$	$J = 1$	$J = 2$
$(\mu/M)B_{3,Z}$	−19.715	−9.857	9.857
$(\mu/M)B_{3,e}$	19.711	9.856	−9.856
$(\mu/M)B_5$	8.099	−4.050	0.810
Δ_3	56.802	28.401	−28.401
$B_{3,Z}^X$	−60.574	−30.287	30.287
$B_{3,e}^X$	56.737	28.369	−28.369
B_5^X	18.739	−9.370	1.874
$-(\mu/M)\Delta E'_{rel}$ [a]	−8.096	4.051	−0.812
$(\Delta E'_{RR})_M$ [b]	1.180	16.788	−10.309
$(\Delta E'_{RR})_X$ [c]	14.902	−11.288	3.792
$\Delta E'_{st}$	0	0.191	0
Total	7.986	9.743	−7.328

[a] $-(\mu/M)\Delta E'_{rel} = -(\mu/M)(B_{3,Z} + B_{3,e} + B_5)$.
[b] $(\Delta E'_{RR})_M = -2(\mu/M)(B_{3,e} + B_5) + \Delta_3$.
[c] $(\Delta E'_{RR})_X = B_{3,Z}^X + B_{3,e}^X + B_5^X$.

The comparison between theory and experiment for the $2\,^3S_1 - 2\,^3P_J$ transition isotope shifts (as opposed to the SIS) is significant because it is sensitive to the difference in nuclear radii. If, for example, $R_{rms}(^7Li)$ is held fixed and $R_{rms}(^6Li)$ is increased, then all the isotope shifts increase together at a rate of 49.5 MHz/fm. Table X lists the calculated contributions to the isotope shift for each state, and compares the results for the transition frequencies with experiment. Although $J = 0$ and 1 are in good agreement, there is a discrepancy for $J = 2$ arising from the SIS anomaly already discussed. If all three measurements are weighted equally, then a least-squares fit reduces the difference in nuclear radii by 0.012 fm from the values assumed in the table to

$$R_{rms}(^6Li) - R_{rms}(^7Li) = 0.15 \pm 0.01 \text{ fm}. \tag{23}$$

This is in excellent accord with nuclear scattering measurements [39], but is nearly an order of magnitude more accurate. An average of the nuclear scattering data gives $R_{rms}(^6Li) = 2.55 \pm 0.04$ fm and $R_{rms}(^7Li) = 2.392 \pm 0.03$ fm for a difference of 0.16 ± 0.05 fm. The above reduction of 0.012 fm for the difference in nuclear radii reduces all the calculated isotope shifts by 0.594 MHz. The differences between theory and experiment for the three transitions then become $-0.45(55)$, $-0.48(67)$, and 0.92(62) MHz, respectively, in place of the differences shown in the last line of Table X.

C. Total transition frequencies and QED shifts

The final step in the analysis is to subtract the known lower-order terms summarized in Eq. (1) from the measured transition frequencies to obtain the residual QED shift. The terms required to calculate E_{low}, together with the QED terms $\Delta E_{L,1}$ and $\Delta E_{L,2}$, are listed in Table XI. The table is in a standardized format with all terms as defined previously for helium [10–12]. In particular, the terms in Eq. (1) correspond to

$$\varepsilon_{0,0} = \Delta E_{nr} - R_M, \tag{24}$$

$$\varepsilon_{0,1}(\mu/M) = \Delta E_M^{(1)}, \tag{25}$$

$$\varepsilon_{0,2}(\mu/M)^2 = \Delta E_M^{(2)}, \tag{26}$$

$$\varepsilon_{2,0}^{(J)}\alpha^2 = \Delta E_{rel} + \Delta E_{st} + \Delta E_{anom}, \tag{27}$$

$$\varepsilon_{2,1}^{(J)}\alpha^2(\mu/M) = (\Delta E_{RR})_M + (\Delta E_{RR})_X, \tag{28}$$

and ΔE_{nuc} is the finite nuclear size correction. Note that, for convenience, the spin-dependent anomalous magnetic moment term ΔE_{anom} is included in $\varepsilon_{2,0}^{(J)}\alpha^2$, even though it is a QED correction of $O(\alpha^3)$. The sum of the above contributions plus ΔE_{nuc} then defines E_{low}.

The QED terms in Table XI are as follows. $\Delta E_{L,2}$

TABLE X. Calculated contributions to the total isotope shifts $\delta E = E(^7\mathrm{Li}^+) - E(^6\mathrm{Li}^+)$. The assumed rms nuclear radii are 2.392 ± 0.03 fm for ^{7}Li and 2.55 ± 0.04 fm for ^{6}Li [39]. Units are MHz.

Contribution	$2\,^3S_1$	$2\,^3P_0$	$2\,^3P_1$	$2\,^3P_2$
δE_{nr}	−9 481.906	−2 373.374	−2 373.374	−2 373.374
$\delta E_M^{(1)}$	−1 504.152	26 124.466	26 124.466	26 124.466
$\delta E_M^{(2)}$	2.616	10.880	10.880	10.880
δE_{rel}	−6.589	1.430	−0.592	0.217
δE_{anom}		0.000	−0.002	0.002
δE_{st}		0.000	−0.032	0.000
$(\delta E_{RR})_M$	3.468	−6.766	−9.363	−4.854
$(\delta E_{RR})_X$	−1.099	−4.320	0.039	−2.470
δE_{nuc}	−6.150	1.432	1.432	1.432
$\delta E_{L,1}$	0.200	0.511	0.511	0.511
$\delta E_{L,2}$	−0.007	−0.003	−0.003	−0.003
Total	−10 993.620	23 754.256	23 753.960	23 756.805
$\delta E(2\,^3P_J - 2\,^3S_1)$		34 747.876	34 747.580	34 750.425
Experiment		34 747.73(55)	34 747.46(67)	34 748.91(62)
Difference		0.15(55)	0.12(67)	1.52(62)

is the accurately known Araki-Sucher electron-electron QED term. The electron-nucleus QED term $\Delta E_{\mathrm{L},1}$ includes a $1/Z$ expansion correction to the Bethe logarithm for the $2\,^3S_1$ state [41], and an asymptotic expansion form of the Bethe logarithm for the $2\,^3P_J$ states [42]. The estimated uncertainties for these terms due to the Bethe logarithm is ±50 MHz for the $2\,^3S_1$ state and ±12 MHz for the $2\,^3P_J$ states. Additional significant figures are quoted in Table XI because the other contributions are known to much higher accuracy. These uncertainties, together with relativistic corrections of $O(\alpha^4 Z^6)$ not included in Table XI [see Eqs. (29)–(32) below], are more than adequate to account for the differences between theory and experiment shown in Table XI. A corresponding table of contributions for ^{6}Li can be obtained by subtracting the isotope shifts listed in Table X from the entries in Table XI.

In view of the uncertainties in the QED terms, the simplest way to summarize the experimental results is to present them in terms of a total QED shift for the transition with ΔE_{low} subtracted. For convenience, the values of ΔE_{low} are tabulated separately in Table XII for both isotopes, and the final QED shifts are given in Table XIII. The slight difference between them for each J reflects the QED isotope shift. The theoretical QED isotope shift from Table X is 0.315 MHz. Adding this amount to the ^{6}Li QED shifts brings them into good agreement with those for ^{7}Li, except for the SIS anomaly of about 1.4 MHz for $J = 2$. With the 0.315 MHz adjustment included, the results for the two isotopes can be averaged, and a further $(2J + 1)$-weighted statistical average performed over J, to obtain a final effective ^{7}Li QED shift of $-37\,429.40 \pm 0.39 \pm 1.5$ MHz. The first uncertainty is the intrinsic accuracy of the experiment, and

TABLE XI. Calculated contributions to the $1s2s\,^3S_1$ and $1s2p\,^3P_J$ state energies of $^7\mathrm{Li}^+$ relative to $^7\mathrm{Li}^{++}(1s)$, with R_M added to ΔE_{nr} and the total. Uncertainties are discussed in the text. The values of the fundamental constants used are $R_M = 3\,289\,584\,688.75(54)$ MHz, $1/\alpha = 137.035\,9895$, and $\mu/M = 7.820\,2031 \times 10^{-5}$. Units are MHz.

Contribution	$2\,^3S_1$	$2\,^3P_0$	$2\,^3P_1$	$2\,^3P_2$
ΔE_{nr}	−728 494 138.87	−182 346 162.33	−182 346 162.33	−182 346 162.33
$\Delta E_M^{(1)}$	9 038.86	−156 989.10	−156 989.10	−156 989.10
$\Delta E_M^{(2)}$	−7.26	−30.18	−30.18	−30.18
ΔE_{rel}	−506 277.79	109 872.59	−45 458.17	16 722.90
ΔE_{anom}		45.39	−217.65	121.51
ΔE_{st}		0	−134.27	0
$(\Delta E_{RR})_M$	−20.84	40.66	56.27	29.17
$(\Delta E_{RR})_X$	6.60	25.96	−.23	14.85
ΔE_{nuc}	45.04	−10.49	−10.49	−10.49
$\Delta E_{L,1}$	30 569.86	−6 838.41	−6 840.89	−6 845.85
$\Delta E_{L,2}$	−185.64	−297.60	−297.60	−297.60
Total	−728 960 970.04	−182 400 343.51	−182 556 084.64	−182 493 447.11
$\Delta E(2\,^3P_J - 2\,^3S_1)$		546 560 626.53	546 404 885.40	546 467 552.93
Experiment		546 560 683.07	546 404 978.80	546 467 657.21
Difference		−56.54	−93.40	−104.28

TABLE XII. Calculated values of $\Delta E_{\rm low}$ for the $2\,^3P_J$–$2\,^3S_1$ transition frequencies of $^6Li^+$ and $^7Li^+$, including $\Delta E_{\rm anom}$. The uncertainties due to the finite nuclear size corrections are ±1.8 MHz for $^6Li^+$ and ±1.3 MHz for $^7Li^+$. Units are MHz.

J	$\Delta E_{\rm low}(^6Li^+)$	$\Delta E_{\rm low}(^7Li^+)$
0	546 598 146.76	546 563 399.20
1	546 442 408.11	546 407 660.84
2	546 505 080.60	546 470 330.49

the second comes from the J-independent finite nuclear radius correction. The intrinsic accuracy of ±11 ppm compares well with the best one-electron measurements in H [2] and He^+ [4].

D. Higher-order relativistic and QED terms

The most important terms not included in the calculations so far are relativistic corrections of $O(\alpha^4 Z^6)$ and $O(\alpha^4 Z^5)$. All terms of this order are automatically included in the "unified method" calculations described previously by Drake [23], together with higher-order extensions in powers of $(\alpha Z)^2$. For low Z, the sum of the above two terms provides an excellent approximation to the $(\alpha Z)^2$ sum. Recently, relativistic configuration interaction calculations by Chen, Cheng, and Johnson [24] have enabled them to subtract the known lower-order contributions and obtain the coefficient of the next term of $O(\alpha^4 Z^4)$. Combining their results with the known lower-order terms [43,44] yields [in the notation of Eq. (1)]

$$\alpha^4\varepsilon_{4,0}(2\,^3P_0) = (Z\alpha)^4[-\tfrac{21}{1024}Z^2 + 0.142\,8908Z - 0.51 + O(Z^{-1})], \tag{29}$$

$$\alpha^4\varepsilon_{4,0}(2\,^3P_1) = (Z\alpha)^4[-\tfrac{43}{3072}Z^2 + 0.056\,8947Z - 0.16 + O(Z^{-1})], \tag{30}$$

$$\alpha^4\varepsilon_{4,0}(2\,^3P_2) = (Z\alpha)^4[-\tfrac{1}{1024}Z^2 - 0.001\,8821Z - 0.003 + O(Z^{-1})], \tag{31}$$

$$\alpha^4\varepsilon_{4,0}(2\,^3S_1) = (Z\alpha)^4[-\tfrac{21}{1024}Z^2 + 0.043\,2232Z - 0.033 + O(Z^{-1})]. \tag{32}$$

TABLE XIII. Experimental values of the QED shift for the $2\,^3P_J$–$2\,^3S_1$ transition of $^6Li^+$ and $^7Li^+$, obtained by subtracting $\Delta E_{\rm low}$ (Table XII) from the measured transition frequencies in Table VIII. Uncertainties do not include those from finite nuclear size corrections (see Table XII). Units are MHz.

J	$\Delta E_{\rm QED}(^6Li^+)$	$\Delta E_{\rm QED}(^7Li^+)$
0	−37 463.86(36)	−37 463.69(42)
1	−37 429.51(44)	−37 429.31(51)
2	−37 422.19(43)	−37 423.39(44)

For $Z = 3$, the $2\,^3P_0$ and $2\,^3P_1$ expansions are not rapidly convergent enough to provide useful results. The poor convergence of the $1/Z$ expansions for low Z explains the apparent disagreements between theory and experiment for fine-structure splittings noted by several authors [19–21,45]. However, for the $2\,^3P_2$ and $2\,^3S_1$ states, there is a better indication of convergence. For these states, the additional shifts are −26 and −134 MHz, respectively. The difference of 108 MHz for the $2\,^3P_2 - 2\,^3S_1$ transition largely cancels the discrepancy of −104.2 MHz between theory and experiment shown in Table XI, leaving a residual discrepancy of only ∼ 4 MHz.

Although the above agreement for the $2\,^3P_2 - 2\,^3S_1$ transition frequency may be partly fortuitous, the small magnitude of the $\alpha^4\varepsilon_{4,0}$ term for the $2\,^3P_2$ state suggests that this state can be taken as a known point of reference to determine the much larger QED shift of the $2\,^3S_1$ state. In addition, the asymptotic expansion used to calculate the two-electron correction to the $2\,^3P$ Bethe logarithm [42] introduces a correction of only −12 MHz in $\Delta E_{L,1}$. Taking this entire correction as the uncertainty, and including the $\alpha^4\varepsilon_{4,0}$ term, the derived experimental QED shift for the $2\,^3S_1$ state of Li^+ is

$$\Delta E_{\rm QED} = 30\,254 \pm 12 \text{ MHz}. \tag{33}$$

The theoretical contributions to the QED shift are as follows. Denote the one-electron Lamb shift (excluding finite nuclear size and relativistic recoil terms) by $\Delta E_L(ns)$, and define $F(ns)$ and d by

$$\Delta E_L(ns) = \frac{Z^4\alpha^3}{\pi n^3}F(ns)\,, \tag{34}$$

$$d = (\pi/Z^3)[\langle\delta(\mathbf{r}_1) + \delta(\mathbf{r}_2)\rangle - 1]\,. \tag{35}$$

Then, in the extended Kabir-Salpeter formalism used in this work, $\Delta E_{L,1}$ for a $1sns$ state is

$$\Delta E_{L,1} = d\Delta E_L(1s) + (1+d)\frac{Z^4\alpha^3}{\pi}\left[\frac{F(ns)-F(1s)}{n^3+1} - \frac{4}{3}\ln\left(1 - \frac{\sigma(n\,^{1,3}S)}{Z}\right)^2\right], \tag{36}$$

where $\sigma(n\,^{1,3}S)$ is a state-dependent screening constant obtained from the second term in a $1/Z$ expansion of the two-electron Bethe logarithm [41]. Although Eq. (36) has been rewritten in a more convenient form for hand calculation, it is exactly equivalent to previous definitions in Refs. [10–12]. To a good approximation for low Z,

$$F(ns) - F(1s) = \tfrac{4}{3}(\beta_{1s} - \beta_{ns}) + \tfrac{4}{3}(\alpha Z)^2\{\ln(\alpha Z)^{-2}[A_{61}(ns) - A_{61}(1s)] \pm 1\} + (\text{reduced mass and recoil terms}), \tag{37}$$

where β_{ns} is the one-electron Bethe logarithm [46], and

TABLE XIV. Contributions to the theoretical QED shift for the $2\,^3S_1$ state of $^7Li^+$. The input data are $\Delta E_L(1s) = 477\,545(50)$ MHz (excluding finite nuclear size and relativistic recoil), $d = 0.062\,043\,69$, $\beta_{1s} = 2.984\,1286$, $\beta_{2s} = 2.811\,7699$, and $\sigma(2\,^3S) = -0.013\,88$ [41]. Units are MHz.

Term	Contribution
$d\Delta E_L(1s)$	29 628 .66 ± 3
$\Delta E_{L,1}(\Delta\beta)$	1 787 .62
$\Delta E_{L,1}(\sigma)$	−861 .74
$\Delta E_{L,1}(\Delta A_{6,1})$	14 .55
Two-electron reduced mass	0 .78
$\Delta E_{L,1}$ subtotal	30 569 .86
$\Delta E_{L,2}$	−185 .64
$\alpha^4\varepsilon_{4,0}$	−134 ±30
Total	30 250 ±30
Experiment	30 254 ±12
Difference	−4 ±32

$$A_{61}(ns) - A_{61}(1s) = -3\ln n + 3\sum_{q=2}^{n} q^{-1} + \tfrac{77}{60}\left(1 - n^{-2}\right) . \qquad (38)$$

The ±1 in Eq. (37) allows for the small n dependence of $A_{6,0}(ns)$ [47]. With the notation $\Delta E_{L,1}(\sigma)$, $\Delta E_{L,1}(\Delta\beta)$, and $\Delta E_{L,1}(\Delta A_{6,1})$ to denote the energy contributions due to the corresponding terms $\sigma(n\,^{1,3}S)$, $\beta_{1s} - \beta_{ns}$, and $A_{61}(ns) - A_{61}(1s)$ in Eqs. (36) and (37), Table XIV shows how the terms add up to give the total theoretical QED shift for the $2\,^3S_1$ state. A further term of $O(\alpha^4 \ln\alpha)$ recently evaluated by Drake *et al.* [48] only affects the singlet states (in LS coupling), and so does not contribute here.

The agreement with experiment at the ±4 MHz level shown in Table XIV is almost certainly due to a fortuitous cancellation of uncalculated terms. However, even if there are further contributions to $\alpha^4\varepsilon_{4,0}$ of ±30 MHz from terms of higher order in $1/Z$ in Eq. (32), the comparison still provides the effective experimental value $\sigma(2\,^3S) = -0.0138(5)$. The corresponding experimental value for He is −0.0132(2) [11,49]. Remembering that the calculated $\sigma(2\,^3S)$ is just the leading term in a $1/Z$ expansion, agreement with the theoretical value −0.013 88 [41] is quite satisfactory in both cases.

E. Comparisons with other measurements

The recent experiment of Rong *et al.* [19] applies heterodyne laser spectroscopy to measure frequency differences among the $^7Li^+$ transitions $2\,^3S(1,5/2) \rightarrow 2\,^3P(J,F)$ with $(J,F) = (0,3/2)$, $(1,5/2)$, and $(2,7/2)$. Our results can be compared with theirs if the $2\,^3S_1$ (3/2-5/2) splitting of 19 187.67(4) MHz from Table IV is first subtracted from the $(1,3/2) \rightarrow (1,5/2)$ measurement in Table II. The results are compared in Table XV with the measurements of Rong *et al.*, together with several older, less accurate measurements. Our values are in good accord with the older data, but are smaller than the measurements of Rong *et al.* by 6.4 ± 2.0 MHz for the (0,3/2)-(1,5/2) interval, and 17.4 ± 1.9 MHz for the (0,3/2)-(2,7/2) interval. The reason for such large discrepancies is not clear. However, the SIS analysis in Sec. III B provides a strong consistency check on our results for the splittings in both $^6Li^+$ and $^7Li^+$. The values of the hyperfine-structure constants they obtain by fitting to their data show corresponding discrepancies from the theoretical values in Table III.

TABLE XV. Comparison of fine-structure intervals for the $^7Li^+$ $2\,^3P$ (J,F) states with previous measurements, as quoted by Rong *et al.* [19]. The present results are obtained by differencing the entries in Table II, with an adjustment of 19 187.67(4) MHz for the hyperfine structure of the $2\,^3S_1$ state. Units are MHz.

Method	$(0,3/2) \rightarrow (1,5/2)$	$(0,3/2) \rightarrow (2,7/2)$
Laser scan[a]	152 049±28	82 681±4
λ meter[b]	152 077±10	82 689±10
Fast beam[c]	152 073±7	82 681±8
Laser heterodyne[d]	152 081.6 ± 2.0[e]	82 704.3 ± 1.9[e]
Present results	152 075.20 ± 0.66	82 686.86 ± 0.58

[a]Bayer *et al.*, Ref. [57].
[b]Schwarzwald, Ref. [58].
[c]Riis *et al.*, Ref. [17].
[d]Rong *et al.*, Ref. [19].
[e]3σ standard deviation.

IV. DISCUSSION

The results of this paper achieve three significant goals. The first concerns the splitting isotope shift. The effect comes almost entirely from the spin-dependent relativistic reduced mass and recoil terms in the Breit interaction, and is free of other theoretical uncertainties (in the absence of hyperfine-structure) down to the ±0.01 MHz level. Agreement between theory and experiment is excellent for the $J = 0 \rightarrow 1$ interval, but there is an apparent discrepancy of 1.39(91) MHz for the $J = 1 \rightarrow 2$ interval. It is not clear whether the anomaly is due to an imperfection in the hyperfine-structure analysis, or to a statistical fluctuation in the experimental data. However, the agreement is good enough to verify that the theoretical contributions to the SIS have been taken into account correctly. A careful analysis of the SIS provides a valuable check on experimental data in high precision experiments of this type.

The second goal concerns the determination of the nuclear radii for ^6Li and ^7Li from the isotope shifts for the $2\,^3P_J$–$2\,^3S_1$ transition. The result $R_{rms}(^6Li) - R_{rms}(^7Li) = 0.15(1)$ fm represents a substantial improvement in accuracy over nuclear scattering measurements on the individual nuclii. Since QED uncertainties largely cancel from the calculated isotope shift, this is a useful technique that can be extended to high-precision measurements on other isotope pairs.

The third and perhaps most significant goal is to subtract the known low-order contributions from the measured transition frequencies to determine the residual

QED shift. The final spin-averaged and isotope-averaged result of $-37\,429.40 \pm 0.39$ MHz (excluding finite nuclear size) for the $^7Li^+$ $2\,^3S$–$2\,^3P$ transition is among the most accurate Lamb shift measurements in the literature. The additional nuclear size uncertainty is ± 1.5 MHz. A full calculation of all QED contributions to this accuracy represents a formidable challenge, and simpler approximation methods are certainly desirable. The extended Kabir-Salpeter formalism used in Sec. III D is rigorously correct only to $O(\alpha^3)$. The extension involved in Eq. (36) is to include all higher-order corrections to the Lamb shift in a one-electron approximation, multiplied by the corrected electron density at the nucleus. The results in Table XIV demonstrate that this captures a great deal of the essential physics. A similar conclusion has recently been reached by Feldman, Fulton, and Ingham [50] by a direct analysis of self-energy terms of $O(\alpha^4)$. The screening parameter $\sigma(2\,^3S) = -0.013\,88$, calculated from the second term in a $1/Z$ expansion of the full two-electron Bethe logarithm [41], appears to be in good accord with experiment for both He and Li^+. However, the full picture will not be clear until all terms of $O(\alpha^4)$ have been rigorously calculated. These include one-loop and two-loop self-energy diagrams, as well as relativistic corrections to the Araki-Sucher terms, and higher powers of $1/Z$ in Eqs. (29)–(32). Work on these problems is just beginning [51,52].

ACKNOWLEDGMENTS

Support for this work was received from the Natural Sciences and Engineering Research Council of Canada (GWFD), the Danish Natural Science Research Council and the Carlsberg Foundation (ER and OP), the Science and Engineering Research Council of the United Kingdom (ER), and the Carnegie Foundation for the Universities in Scotland (AGS).

[1] W. E. Lamb, Jr. and R. C. Retherford, Phys. Rev. **72**, 241 (1947).
[2] S. R. Lundeen and F. M. Pipkin, Metrologia **22**, 9 (1986).
[3] See, for example, G. W. F. Drake, Adv. At. Mol. Phys. **18**, 399 (1982).
[4] A. van Wijngaarden, J. Kwela, and G. W. F. Drake, Phys. Rev. A **43**, 3325 (1991).
[5] R. S. Van Dyck, Jr., P. B. Schwinberg, and H. G. Dehmelt, in *Atomic Physics 9*, edited by R. S. Van Dyck, Jr. and N. E. Fortson (World Scientific, Singapore, 1984), p. 53.
[6] H. Hellwig, R. F. C. Vessot, M. W. Levine, P. W. Zitzewitz, D. W. Allan, and D. J. Glaze, IEEE Trans. Instrum. Meas. **IM-19**, 200 (1970).
[7] L. Essen, R. W. Donaldson, M. J. Bangham, and E. G. Hope, Nature **229**, 110 (1971).
[8] J. Sapirstein, in *Quantum Electrodynamics*, edited by T. Kinoshita (World Scientific, Singapore, 1990), pp. 580–586.
[9] F. Schmidt-Kaler, D. Leibfreid, M. Weitz, amd T. W. Hansch, Phys. Rev. Lett. **70**, 2261 (1993).
[10] G. W. F. Drake and Z.-C. Yan, Phys. Rev. A **46**, 2378 (1992).
[11] G. W. F. Drake, in *Long-Range Casimir Forces: Theory and Recent Experiments in Atomic Systems*, edited by F. S. Levin and D. A. Micha (Plenum, New York, 1993).
[12] G. W. F. Drake, Adv. At. Mol. Opt. Phys. (to be published).
[13] Y. Accad, C. L. Pekeris, and B. Schiff, Phys. Rev. A **4**, 516 (1971).
[14] J. D. Morgan III, in *Relativistic, Quantum Electrodynamic, and Weak Interaction Effects in Atoms*, AIP Conf. Proc. No. 189, edited by W. Johnson, P. Mohr, and J. Sucher (AIP, New York, 1989), p. 123.
[15] M. Englert, J. Kowalski, F. Mayer, R. Neumann, S. Noehte, R. Schwarzwald, H. Suhr, K. Winkler, and G. zu Putlitz, Appl. Phys. **B 28**, 81 (1982).
[16] R. A. Holt, S. D. Rosner, T. D. Gaily, and A. G. Adam, Phys. Rev. A **22**, 1563 (1980).
[17] E. Riis, H. G. Berry, O. Poulsen, S. A. Lee, and S. Y. Tang, Phys. Rev. A **33**, 3023 (1986).
[18] J. Kowalski, R. Neumann, S. Noehte, K. Scheffzek, H. Suhr, and G. zu Putlitz, Hyp. Int. **15/16**, 159 (1983); A similar analysis of singlet-triplet mixing in the S states of Li^+ was performed by J. Kowalski, R. Neumann, S. Noehte, H. Suhr, G. zu Putlitz, and R. Herman, Z. Phys. A **313**, 147 (1983).
[19] H. Rong, S. Grafström, J. Kowalski, G. zu Putlitz, W. Jastrzebski, and R. Neumann, Z. Phys. D **25**, 337 (1993).
[20] T. J. Scholl, R. Cameron, S. D. Rosner, L. Zhang, and R. A. Holt, Phys. Rev. Lett. **71**, 2188 (1993).
[21] T. Dinneen, N. Berrah-Mansour, H. G. Berry, L. Young, and R. Pardo, Phys. Rev. Lett. **66**, 2859 (1991).
[22] H. G. Berry, R. W. Dunford, and A. E. Livingston, Phys. Rev. A **47**, 698 (1993).
[23] G. W. F. Drake, Can. J. Phys. **66**, 586 (1988).
[24] M. H. Chen, K. T. Cheng, and W. R. Johnson, Phys. Rev. A **47**, 3692 (1993).
[25] S. Gerstenkorn and P. Luc, *Atlas du spectra d'absorption de la molécule de l'iode (14 800–20 000 cm^1)* (Editions du CNRS, Paris, 1978).
[26] G. P. Barwood and W .R. C. Rowley, *ibid.* **20**, 19 (1984); G. P. Barwood, W. R. C. Rowley, and P. T. Woods, *ibid.* **20**, 157 (1984).
[27] T. J. Quinn, Metrologia (to be published). The absolute frequency recommended for the I_2 stabilized He-Ne laser is $473\,612\,214.705 \pm 0.025$ MHz.
[28] A. R. Edmonds, *Angular Momentum in Quantum Mechanics* (Princeton University, Princeton, 1960), Chap. 7.
[29] M. Mizushima, *Quantum Mechanics of Atomic Spectra and Atomic Structure* (Benjamin, New York, 1970), Chap. 9.
[30] L. Hambro, Phys. Rev. **175**, 31 (1968); K. Aashamar and L. Hambro, J. Phys. B **10**, 553 (1977).
[31] E. A. Hinds, J. D. Prestage, and F. M. Pichanick, Phys. Rev. A **32**, 2615 (1985); **32**, 2712 (1985).
[32] A. Beckmann, K. D. Böklen, and D. Elke, Z. Phys. **270**,

173 (1974).
[33] P. Raghavan, At. Data Nucl. Data Tables **42**, 189 (1989).
[34] O. Lutz, Z. Naturforsch. **23a**, 1202 (1968).
[35] D. Sundholm, P. Pyykkö, L. Laaksonen, and A. J. Sadlej, Chem. Phys. Lett. **112**, 1 (1984).
[36] A. Weller, P. Egelhof, R. Čaplar, O. Karban, D. Krämer, K.-H. Möbius, Z. Moroz, K. Rusek, E. Steffens, G. Tungate, K. Blatt, I. Koenig, and D. Fick, Phys. Rev. Lett. **55**, 480 (1985).
[37] A. H. Wapstra and G. Audi, Nucl. Phys. A **432**, 1 (1985).
[38] H. Grotch and D. R. Yennie, Rev. Mod. Phys. **41**, 350 (1969).
[39] C. W. de Jager, H. de Vries, and C. de Vries, At. Data Nucl. Data Tables **14**, 479 (1974).
[40] P. Zhao, J. R. Lawall, and F. M. Pipkin, Phys. Rev. Lett. **66**, 592 (1991).
[41] S. P. Goldman and G. W. F. Drake, J. Phys. B **17**, L197 (1984).
[42] S. P. Goldman and G. W. F. Drake, Phys. Rev. Lett. **68**, 1683 (1992).
[43] G. W. F. Drake, Nucl. Instrum. Methods Phys. Res. **B 9**, 465 (1985).
[44] P. Mohr, Phys. Rev. A **32**, 1949 (1985).
[45] G. W. F. Drake, Nucl. Instrum. Methods **202**, 273 (1982). See also G. W. F. Drake, in *Atomic Physics 8: Proceedings of the Eighth International Conference on Atomic Physics*, edited by I. Lindgren, A. Rosén, and S. Svanberg (Plenum, New York, 1983), pp. 191–193.
[46] G. W. F. Drake and R. A. Swainson, Phys. Rev. A **41**, 1243 (1990).
[47] P. J. Mohr and Y.-K. Kim, Phys. Rev. A **45**, 2727 (1992); P. J. Mohr, Ann. Phys. (N.Y.) **88**, 26 (1974); **88**, 52 (1974).
[48] G. W. F. Drake, I. B. Khriplovich, A. I. Milstein, and A. S. Yelkhovsky, Phys. Rev. A **48**, R15 (1993).
[49] G. W. F. Drake, Nucl. Instrum. Methods Phys. Res. **B 31**, 7 (1988).
[50] G. Feldman, T. Fulton, and J. Ingham, Ann. Phys. (N.Y.) **219**, 1 (1992); A. Devoto, G. Feldman, and T. Fulton (unpublished).
[51] S. A. Blundell, P. J. Mohr, W. R. Johnson, and J. Sapirstein, Phys. Rev. A **48**, 2615 (1993).
[52] Z.-C. Yan and G. W. F. Drake (unpublished).
[53] W. L. Williams, Ph.D. thesis, Yale University, 1966.
[54] S. D. Rosner and F. M. Pipkin, Phys. Rev. A **1**, 571 (1970). See also Ref. [40].
[55] H. A. Schuessler, E. N. Fortson, and H. G. Dehmelt, Phys. Rev. **187**, 6 (1969).
[56] A. P. Stone, Proc. Phys. Soc. London **81**, 868 (1963).
[57] R. Bayer, J. Kowalski, R. Neumann, S. Noehte, H. Suhr, K. Winkler, and G. zu Putlitz, Z. Phys. A **292**, 329 (1979).
[58] R. Schwarzwald, Diploma thesis, University of Heidelberg, 1982.